Fire Performance and Post-Fire Mechanical Properties of Polymer Composites Coated with Hybrid Carbon Nanofiber Paper

Jinfeng Zhuge,[1] Jihua Gou,[1] Ruey-Hung Chen,[1] Aixi Zhou,[2] Ziqing Yu[2]

[1]*Department of Mechanical, Materials and Aerospace Engineering, University of Central Florida, Orlando, Florida 32816*
[2]*Department of Engineering Technology, University of North Carolina at Charlotte, Charlotte, North Carolina 28223*

Received 22 February 2011; accepted 23 May 2011
DOI 10.1002/app.34965
Published online 30 September 2011 in Wiley Online Library (wileyonlinelibrary.com).

ABSTRACT: In this study, glass fiber reinforced polyester composites were coated with carbon nanofiber/clay/ammonium polyphosphate (CCA) paper and carbon nanofiber/exfoliated graphite nanoplatelets/ammonium polyphosphate (CXA) paper. The composites were exposed to a heat flux of 35 kW/m^2 during the cone calorimeter testing. The testing results showed a significant reduction in both heat release rates and mass loss rates. The peak heat release rate (PHRR) of CCA and CXA composite samples in the major decomposition period are 23 and 34% lower than the control sample, respectively. The time to reach the PHRR for the CCA and CXA composite samples are $\sim$ 125% longer than the control sample. After the composite samples were exposed to heat for different time periods, their post-fire mechanical properties were determined by three-point bending testing. The three-point bending testing results show that the composite samples coated with such hybrid papers exhibit more than 20% improvement in mechanical resistance at early stages of combustion. The mechanism of hybrid carbon nanofiber paper protecting the underlying laminated composites is discussed.
 J Appl Polym Sci 124: 37–48, 2012

Key words: carbon nanofiber paper; polymer composites; post-fire; mechanical behavior

INTRODUCTION

During recent years, extensive research has been performed to reduce natural vulnerabilities of polymers and polymer-based materials to fire.[1] Among this research, nano-sized and intumescent fire retardants have drawn special attention, owing to their environmental friendly nature and efficiency in reducing both heat release and toxic gases.[2] In addition, the incorporation nano-sized particles into polymer matrices of fiber reinforced polymers (FRP) can significantly improve the mechanical properties of materials.[3–5]

Carbon nanotubes have been extensively studied as a new type of fire retardants. Kashiwagi et al. found that by dispersing only 0.5 wt % of single-walled carbon nanotubes (SWNTs) into PMMA, the nanocomposite exhibited more than 50% reduction in peak heat release rate. They proposed that the well-dispersed SWNTs would promote the nanocomposite to form a char layer that had a continuous and compact network structure. The char layer acted as protective barrier, resisting heat convection and radiation and reducing mass (fuel) flow to feed flame.[6] With the improvement of fire resistant behavior of polymers, many studies have been carried out to evaluate the in-fire and post-fire mechanical behavior of fire-retarded FRP.[7–10] One of the models to study the post-fire mechanical properties of marine composites was proposed by Mouritz et al. in which the structure of post-fire FRP was modeled as charred and unburnt layers. The post-fire mechanical properties depend on the depth of the charred layer which can be approximately determined from the duration of combustion. The duration of the combustion essentially depends on the time to ignition (TTI), provided that the total period of exposure for the samples is the same.

$$d_c \approx [a(t - t_c)]^{1/2} \tag{1}$$

where d_c is the char thickness, t is the total heat exposure time, t_c is the TTI, and a is an empirical constant.[10,11] Since it is assumed that there is no mechanical resistance for charred material, the model predicted that the effective elastic modulus, E_{eff}, of a post-fire composite sample is (bending condition):

$$E_{\text{eff}} = E_v \cdot \frac{(d - d_c)^3}{d^3} \tag{2}$$

where E_v is the elastic modulus of the virgin material and d is the thickness of the sample. Generally,

Correspondence to: J. Gou (jihua.gou@ucf.edu).
Contract grant sponsor: Office of Naval Research; contract grant number: N00014-09-1-0429.
Contract grant sponsor: National Science Foundation Nanomanufacturing Program; contract grant number: CCMI-0757302.

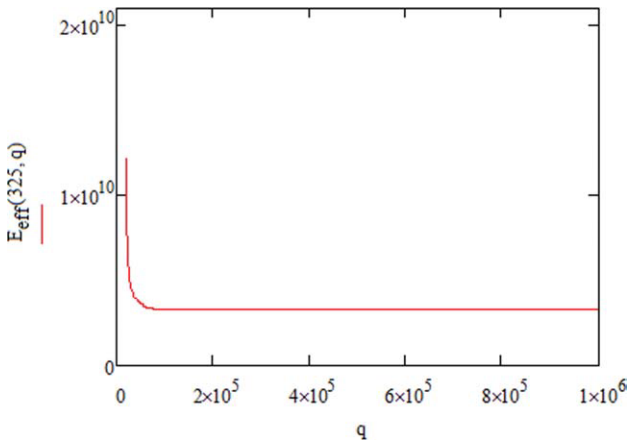

Figure 1 Effect of heat flux on the effective elastic modulus based on the two-layer model proposed by A.P. Mouritz et al. (Re-drawn by Mathcad). [Color figure can be viewed in the online issue, which is available at wileyonlinelibrary.com.]

this model works well to predict the post-fire mechanical properties. However, one unfavorable result of Mouritz's model is that the effective modulus will become independent of heat flux after it reaches certain value for the same heat exposure time, as shown in Figure 1. This error possibly comes from the assumption that the elastic modulus of the charred layer is zero. The SEM images of the char attached to glass fibers suggest that it could be more accurate if the mechanical properties of the char are modeled to decrease gradually. More detailed discussions will be given in the analysis of the char morphology.

In this study, carbon nanofibers (CNFs) were used as the primary material to make hybrid nanopapers which served as a high quality "pre-existing char layer" when they were coated to the surface of FRP to improve the fire resistance of the composites.[12–14] New types of highly effective hybrid nanopapers were developed in this study. APP particles were introduced into the CNF paper. The particles would serve as a blow agent that was expected to lower the through-thickness thermal conductivity of the nanopaper and to initiate the creation of char that would protect the underlying polymer from fire damage. The platelet structures of clay and exfoliated graphite nanoplatelets (xGnP) were introduced into the CNF papers. These particles was used to lower the

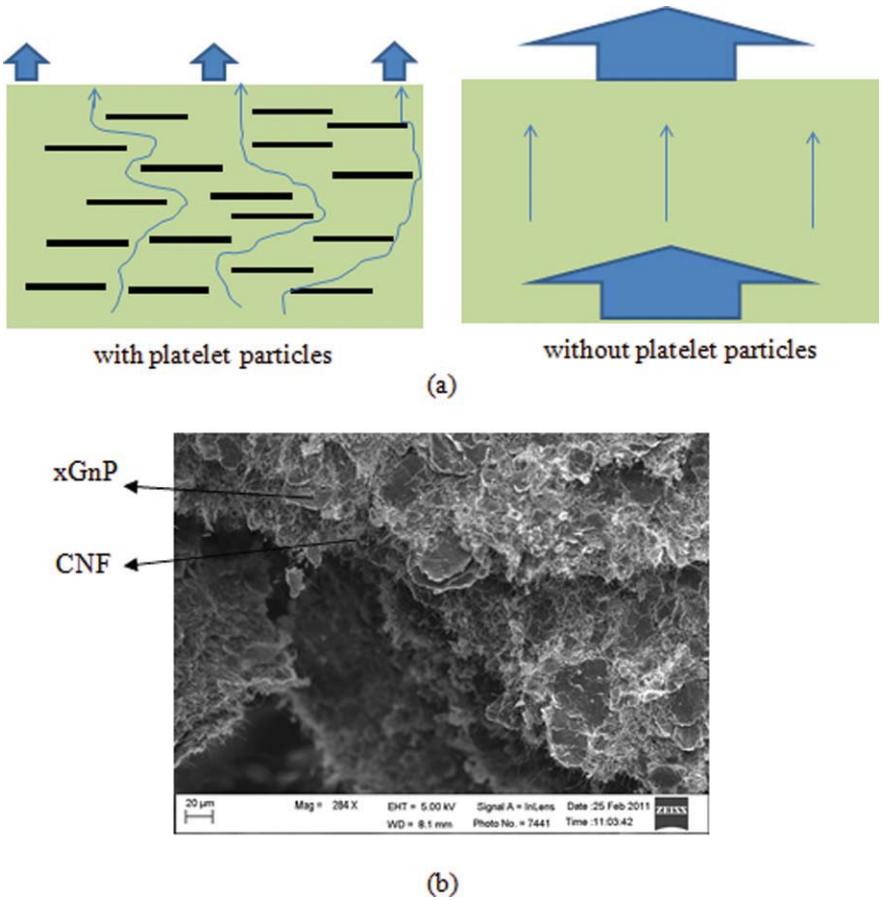

Figure 2 (a) The presence of platelet particles inhibits the diffusion of decomposed resin; (b) The actual cross-section structure of hybrid nanopaper containing xGnP. [Color figure can be viewed in the online issue, which is available at wileyonlinelibrary.com.]

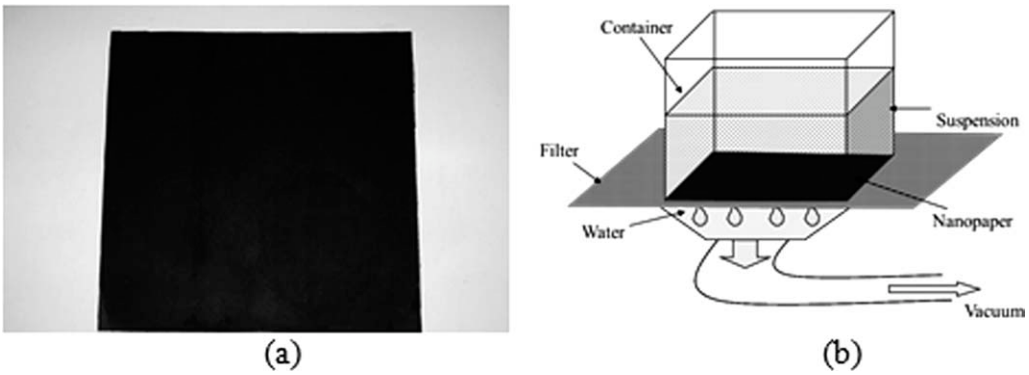

Figure 3 (a) Digital image of as-made nanopaper, and (b) Vacuum-assisted filtration system.

permeability of the pre-existing char layer so that the path of decomposed polymer (fuel) become torturous, as shown in Figure 2(a). As a result, the nanopapers would serve as barrier to prevent the decomposed fuel from feeding the flame [Fig. 2(b)]. The purpose to use xGnP, besides the above reason, was to take advantage of their anisotropic thermal conductivity ($K_{\parallel} = 3000$ W/m; $K_{\perp} = 6$ W/m)[15] so that heat could be easily dissipated during heat transfer. In this study, the fire performance of the nanocomposites was evaluated by cone calorimeter testing. Since the tensile and compressive properties of the composites mostly is dominated by glass fibers which have no damage after fire and the mechanical properties of matrix, respectively, and since the flexural modulus represents the combined effect of glass fibers and polymer matrix, the post-fire mechanical properties were evaluated by three-point bending test in this study.

EXPERIMENTAL

Materials

Vapor grown carbon nanofibers (Polygraf III PR25-HHT) were produced from Applied Sciences, Inc. with diameters of around 80nm and surface area of about 50 m^2/g. The Cloisite Na^+ clay was the pure and nonmodified form of montmorillonite clay which was obtained from Southern Clay Products. According to the product specifications, 90% by volume of dry particles have sizes that less than 13 μm. The X-ray result in [001] direction is 11.7 Å. The exfoliated graphite nano platelets (xGnP) were obtained from XG Sciences with a thickness of 5–15 nm. The traditional flame retardant, ammonium polyphosphate (AP423) was supplied by Clariant International. The glass fiber mats (GF) was supplied from Composites One with a surface density of 800 g/m^2 and an average thickness of 0.85 mm. The pre-promoted, thixotropic, orthophthalic type of unsaturated polyester resin supplied by PolyGrad (product code: GP100P; density: 1.1 g/cm^3; heat deflection temperature: 75°C) was used as matrix material for laminated composites with the methyl ethyl ketone (MEK) peroxide as hardener at a weight ratio of 100 : 1.

Processing of hybrid nanopapers and nanocomposites

The as-received CNF, Clay, and APP or CNF, xGnP, and APP powders were mixed together at a weight ratio of 5/1/9 and dispersed in 1000 mL of distilled water with the aid of surfactant Triton-X100 (3–5 drops). It was worthy to note that the weight ratio of CNF/Clay/APP = 5/1/9 was chosen based on our previous experiment in which the fire retardancy of such type of nanopaper was the best.[16] For comparison, the weight ratio of CNF/xGnP/APP was selected to be 5/1/9. The mixture was then sonicated with a Misonix *S*-3000 for 15 min at a power of 60–80 W. After the suspension was well dispersed, the nanopapers [Fig. 3(a)] were fabricated by filtering the suspension through a vacuum system shown in Figure 3(b). It should be noted that the time to fabricate the nanopapers containing clay was much longer than those nanopapers containing xGnP due to the lower permeability.

The as-made nanopapers were dried at 120°C and coated to the surface of the FRP during resin transfer molding (RTM) process. The composition of the hybrid nanopapers and nanocomposites is shown in Table I.

Characterization and evaluation

Cone calorimeter test

The evaluation of flame retardant performance of the nanocomposites was conducted using a cone calorimeter at an incident heat flux of 35 kW/m^2 in accordance with ISO 5660-1 standard. The composites were cut into discs with the diameter of 75mm. The thickness of the samples was roughly 4 mm. The volume and weight fraction of resin were 70 and

TABLE I
Composition of Hybrid Nanopapers and Nanocomposites

Nanocomposites sample ID	Contents (wt %)			Weight ratios of particles in the nanopaper
	GF	Resin	Nanopaper	
Control	50.6	49.4	0	No paper
CCA serials	49.3	47.6	3.1	CNF/Clay/APP = 5/1/9
CXA serials	51.0	45.8	3.2	CNF/xGnP/APP = 5/1/9

50%, respectively. The nontesting surfaces of the composite samples were wrapped in aluminum foil prior to the cone calorimeter test. All the samples were evaluated in a horizontal position with the surfaces coated with nanopaper when applicable, directly exposed to the heat flux during cone calorimeter tests. The experiments were repeated three times for each sample, and the results were reproducible to within 10%. The cone data reported in this study was an average of the three replicated tests. Additionally, the composites panels were cut into 130 mm by 25 mm strips. Those samples were exposed to heat using the cone calorimeter equipment with the same heat flux. The exposure times of the samples were 20, 60, 100, 150, 200, 250, and 300 s.

Thermogravimetric analysis

The TGA instrument used in this study was TGA-Q500 from TA Instruments, USA. The characterization of the hybrid nanopapers infused with the polyester resin was conducted in nitrogen atmosphere at a flow rate of 40 mL/min and a heating rate of 10°C/min. The sample size of specimens was ~ 10 mg which was obtained by knocked off the surface of the nanocomposites composed of resin and hybrid nanopaper. The nitrogen atmosphere was chosen to model the degradation of polymer within the composite material, i.e., there was unlikely oxygen presented inside the sample during combustion process.

Post fire three-point bending test

Post-fire flexural properties of the samples were evaluated by three-point bending method using an INSTRON 5582 universal testing machine. In according with ASTM D790-10, the support span was 76 mm and the rate of crosshead motion for these samples was 2.4 mm/min. The testing would stop if either the deflection of the centerline of the specimen at the middle of the support span reached 12 mm or there was a dramatic drop in the load-deflection curve. The tangent modulus of elasticity was calculated by[17]:

$$E_B = \frac{L^3 \cdot m}{4 \cdot b \cdot d^3} \quad (3)$$

where: E_B is the modulus of elasticity in bending, L is the support span, b is the width of beam tested, d is the depth of beam, and m is the slope of the tangent to the initial straight line portion of the load-deflection curve. During the bending test, the surface against the support experienced the largest stress. It is possible that even though two samples might have some difference in damaged surface, the undamaged unexposed surface against the support could make the difference in overall mechanical property negligible. This result is unlikely to occur if the damaged surface experiences the largest stress. Therefore, the surface of the samples that exposed to heat flux was placed against the support points as shown in Figure 4.

Temperature measurement

Since the CCA samples and CXA samples have similar fire performance. The temperature history of the unexposed surface of only the CXA serial samples during 35 kw/m^2 cone test was recorded by using K type thermocouples GG-K-24-SLE supplied from Omega Engineering Inc.

Scanning electron microscopy

The hybrid nanopapers, char materials of the samples after cone calorimeter test, and unburnt and partially degraded resin were sputter-coated with a conductive gold layer. They were then analyzed by

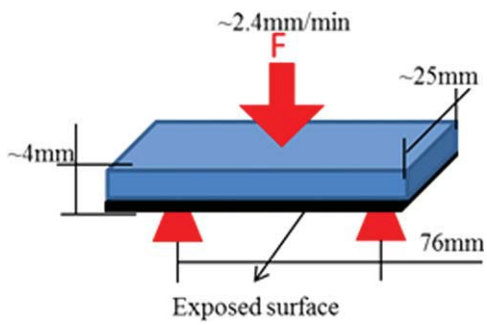

Figure 4 Experimental setup of the composite sample for three-point bending test. [Color figure can be viewed in the online issue, which is available at wileyonlinelibrary.com.]

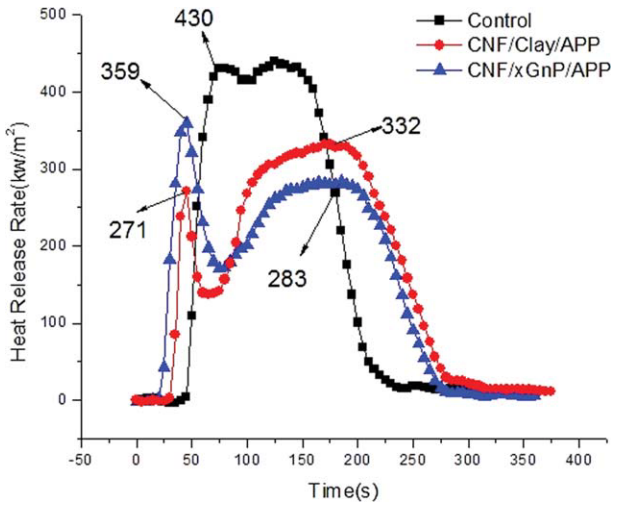

Figure 5 Heat release rate of the samples. [Color figure can be viewed in the online issue, which is available at wileyonlinelibrary.com.]

a Zeiss Ultra -55 SEM machine with target EHT value of 5 kV and working distance of 4–7 mm.

RESULTS AND DISCUSSION

Heat release rate, time to ignition, and mass loss

The HRR curves of these three groups of composite samples are shown in Figure 5 and summarized in Table II. By integrating the heat release rate through time, the heat release before 180 s for the Control, CNF/Clay/APP (CCA), and CNF/xGnP/APP (CXA) samples are 90, 63, and 69% of the total heat release (THR), respectively. Initially, the control samples have the highest HRR and become the lowest after 180 s. Such drop in HRR for the control samples is due to the fact that the polymer matrices have almost been consumed up. Since the only difference between the control samples and the paper-coated samples is that there are thin layer coatings on the surface of the paper-coated samples. Therefore, they have the same amount of the polymer. As a result, when the control sample burns dramatically during the 0–180 s period (90% of THR), it has less fuel to consume in the later combustion stage. Consequently, it can be concluded that in general, the samples coated with hybrid nanopapers exhibited better fire retardancy than the control samples.

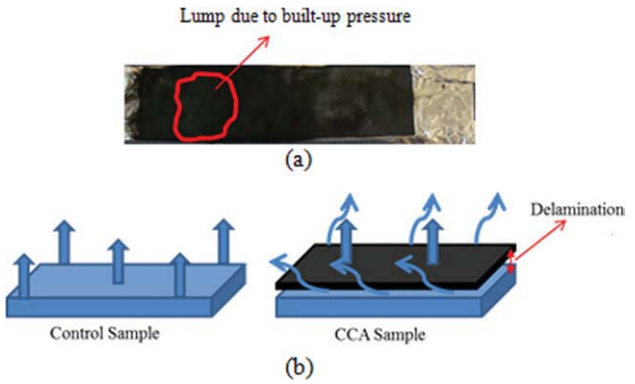

Figure 6 (a) The built-up pressure of the nanopaper results in delamination and (b) mechanism of permeability-related ignition, arrows indicates the decomposed fuel. [Color figure can be viewed in the online issue, which is available at wileyonlinelibrary.com.]

It is interesting to note that there are two peaks for the samples coated with hybrid nanopapers while there is only one peak for the control samples. The first and second peaks of the CCA samples are 37 and 23% lower than that the peak heat release rate (PHRR) of the control samples. The first and second PHRR of CXA are 17 and 34% lower than that the PHRR of the control samples. The first peaks of the paper-coated samples come from the ignition of the samples. The second peak of paper-coated samples and the peaks of the control samples all appear in the highest "platform" of their heat release rate curve. The "platform" represents the major decomposition of the composites since the heat release during the platform period (less than one third of the total combustion process) for the Control, CCA and CXA samples take 66, 58, and 51% of the THR of the samples, respectively. It can be seen that the second PHRR of the CCA and CXA samples appear at 170 and 185 s, respectively. Much later than the control samples whose peaks occur at about 80 s. As shown in Figure 5, immediately following the first peak of the paper-coated samples a dramatic decrease in HRR occurs. It is unlikely that the drop is due to the complete consumption of composite material. Rather it is due to the formation of the protective char layer. In fact, the introduction of the hybrid nanopaper is intentionally designed to serve as a pre-existing char layer and to prompt the formation of the protective char. The occurrence of

TABLE II
Summary of Cone Calorimeter Data

Sample ID	THR (MJ/m^2)	THR (0 ~ 180 s) (MJ/m^2)	THR ("platform") (MJ/m^2)	First PHRR (kw/m^2)	Second PHRR (kw/m^2)	Time to second PHRR (s)
Control	57.9	51.7	38.4	/	430	80
CCA	59.5	37.3	34.4	271	332	170
CXA	55.5	38.2	28.2	359	283	185

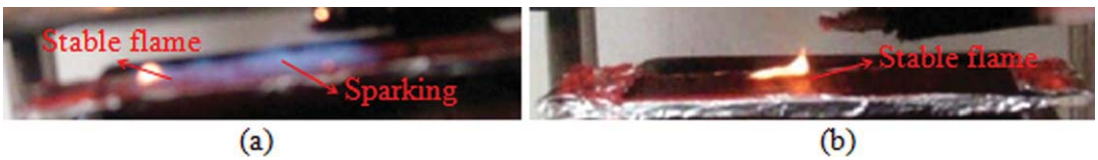

Figure 7 The flame pattern on the surface of the samples just after ignition: (a) control sample and (b) nanopaper-coated sample. [Color figure can be viewed in the online issue, which is available at wileyonlinelibrary.com.]

the second peaks could be attributed to the cracking of the char layer near the end of combustion process. It is more desirable to lower down the value of the second peak since most of the materials decompose around this peak.

Since we expect the protective char to be formed at the early stage, the ignition time of the paper-coated samples is shorter than the control samples, as shown in Figure 5, and the first PHRR occurs when the samples catch fire. The shortened ignition time of CXA serial samples is attributed to high content of carbon particles in the hybrid nanopaper, which easily absorb energy and conduct heat. The reason for the first peaks in HRR curves (or ignition) of the CCA serial samples, besides the effect of high carbon content, could also be attributed to the extremely low permeability, as mentioned in experimental section of this study, which results in the build-up of pressure between nanopaper and underlying structure [lump in Fig. 6(a)]. Consequently, the delamination of nanopapers occurs and the gas bursting out from the gap reaches the critical fuel concentration value that eventually leads to ignition [as shown in Fig. 6 (b)]. Therefore, the peak occurs due to the large amount of newly freed fuel igniting.

When the samples continuously burn, the resin within the nanopaper will be consumed up, and the protective char layer forms. Then, since the flame is maintained by the fuel that comes from the underlying polymer decomposition, the permeability of the nanopaper affects the long term HRR, i.e., the lower the permeability, the less the fuel pass through the protective layer, thus the lower the HRR. This is indicated as a dramatic drop in the HRR immediately after the first peak, then a relatively low HRR maintained after the drop. As shown in Figure 7(a), the lack of protection of the control sample leads to a large area of sparking appears before and immediately after ignition, which is barely observed with the sample coated with the nanopaper [Fig. 7(b)]. The large sparking area of the control sample indicates that large amount of fuel present. It is important to note that despite the HRR of the paper-coated sample being lower than the control sample,

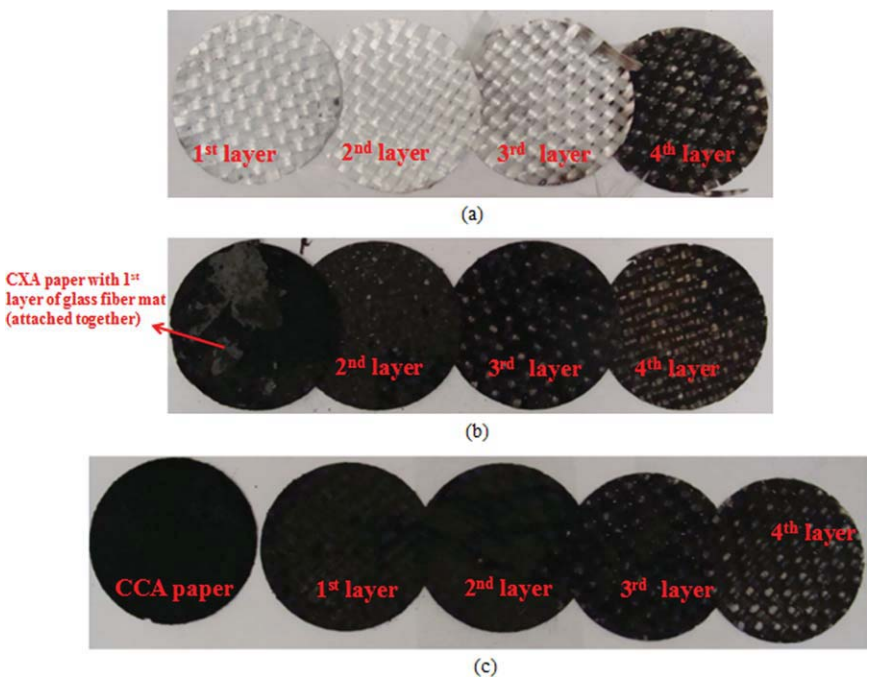

Figure 8 The char material collected after cone calorimeter test (1st layer is more close to the heat flux than the successive layers): (a) control sample, (b) CXA sample, and (c) CCA sample. [Color figure can be viewed in the online issue, which is available at wileyonlinelibrary.com.]

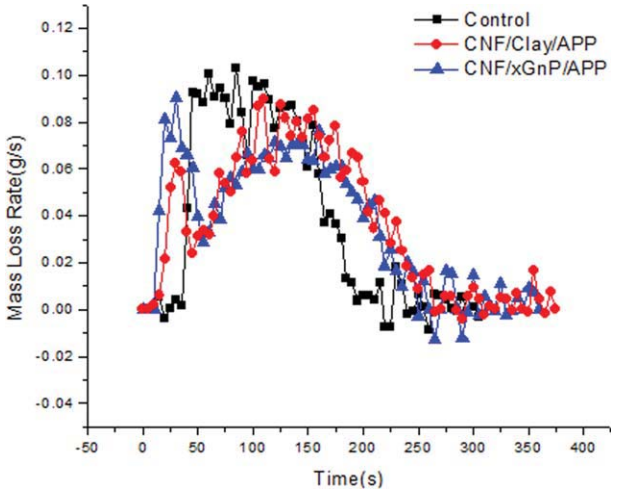

Figure 9 Mass loss rate of the samples. [Color figure can be viewed in the online issue, which is available at wileyonlinelibrary.com.]

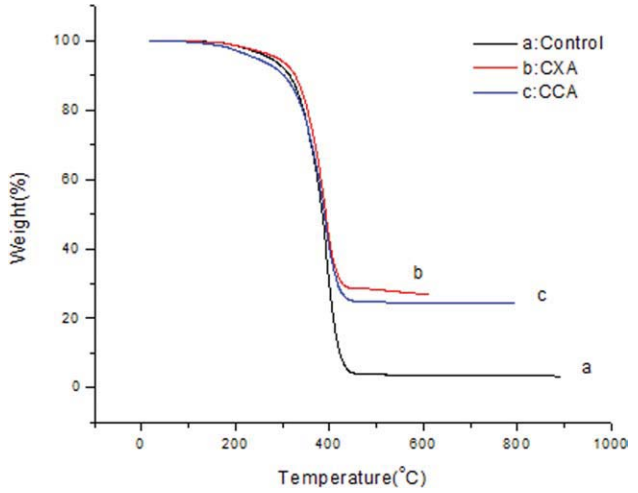

Figure 11 TGA data of the samples. [Color figure can be viewed in the online issue, which is available at wileyonlinelibrary.com.]

the total heat release (THR) of the three groups of samples are similar (about 57 MJ/m^2) which indicates that small quantity of the hybrid nanopaper does not affect the THR of the material and large quantity of traditional FR is indispensible if attempting to lower the value and achieve V-0 rating in the UL-94 test.[1–2]

The CCA type of nanopaper has much lower permeability of the CXA nanopaper, which causes the relatively lower HRR (less fuel penetrates the coating) during the first peak period and the lump of the nanopaper [Fig. 6(a)]. However, the HRR of the CCA samples becomes much higher than the CXA samples after that. This phenomenon can be attributed to the complete detachment of the coating from the samples coated with the CCA papers. When the coating is detached from the underlying glassfiber mat, the barrier effect of the coating will be compromised. As shown in Figure 8, the CCA coating is already detached from the underlying glassfiber mat after cone calorimeter test while the CXA paper is still attached to the 1st layer of glassfiber mat. Furthermore, when there is no coating applied to the control sample, all the polymer matrix is completely burnt without turning into char, leaving the white original glassfiber mats behind. However, for the paper-coated samples, the glassfiber mats catch more char when they are getting closer to the surface coating since the coating prevents the degraded fuel to feed the surface flame during the cone calorimeter test.

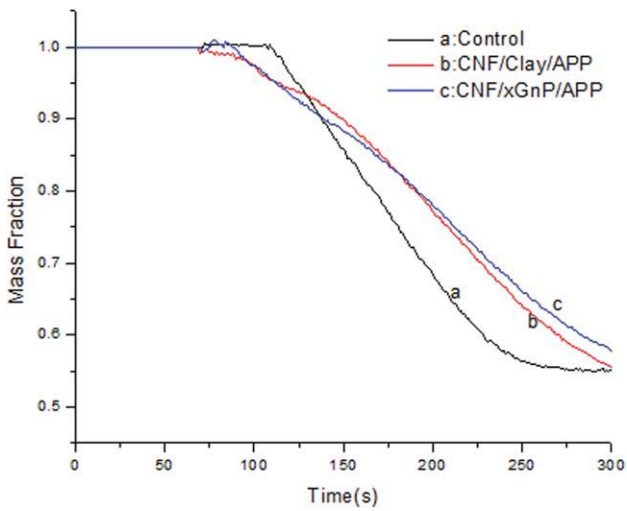

Figure 10 Mass remaining of the samples during cone calorimeter test. [Color figure can be viewed in the online issue, which is available at wileyonlinelibrary.com.]

Figure 9 shows the mass loss rate of the composite samples. The curves closely follow the HRR curves, i.e., the moment of the highest rate of mass loss is the same time when PHRR appears. Within the first 50 s the mass loss rates of the paper-coated sample increase and then decrease dramatically. The phenomenon suggests that the protective char layers have effectively lowered the decomposed fuel available to feed the flame.

Figure 10 shows the change of mass ratios of the samples while they are exposed to heat flux. The mass ratios are calculated from normalizing the mass of the samples during the test by their initial weight. The hybrid nanopapers protect the samples

TABLE III
Thermal Stability of the Samples

TGA sample ID	$T_{-5\ wt\ \%}$ (°C)	Char (wt %) @ 600°C
Control	274	3.7
CCA	242	24.5
CXA	289	27.1

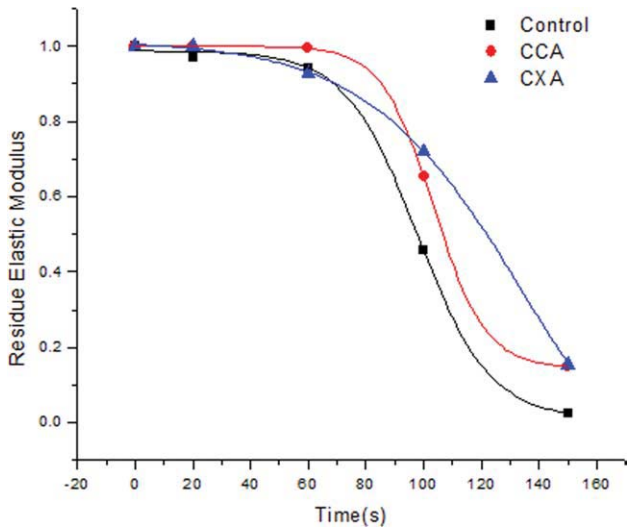

Figure 12 Residual elastic modulus of the samples after exposing to heat flux at different time. [Color figure can be viewed in the online issue, which is available at wileyonlinelibrary.com.]

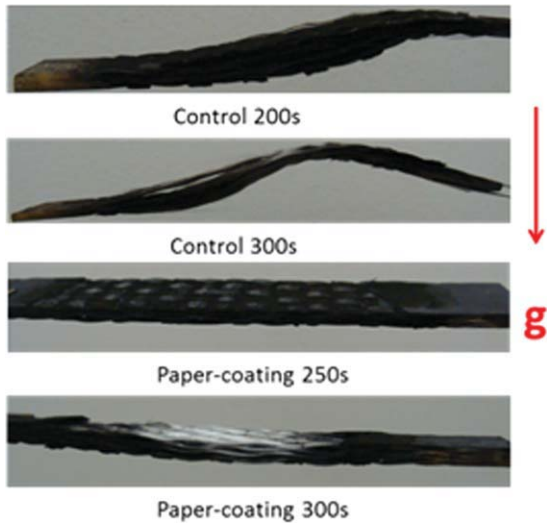

Figure 13 Comparison of self-weight sustaining ability. [Color figure can be viewed in the online issue, which is available at wileyonlinelibrary.com.]

in fire scenario by means of retaining the weight of samples. It can be seen that the mass of paper-coated samples begins to drop earlier than the control sample due to the reduced ignition time. However, since these samples are well protected by char layers, the decrease in mass is much slower than the control samples.

Thermal stability

The thermal stability of the hybrid nanopapers is one of the important factors that affect the fire performance of the nanocomposites. TGA is the most widely used technique to evaluate the thermal stability of various polymer composites. As shown in Figure 11 and Table III, the temperatures at 5% weight loss, which are defined as the initial decomposition temperatures, for the Control, CXA and CCA samples are 274, 289, and 242°C, respectively. The residual at 600°C for the above three samples are 3.65, 27.1, and 24.53%, respectively. Therefore the incorporation of nanopaper into resin results in very high percentage of char yielding which can be attributed to the extremely high thermal stability of the CNF and xGnP particles. Compare to the CCA sample, the higher initial decomposition temperature and char residues for the CXA sample can be attributed to the fact that the layered graphite can prevent the oxygen diffuse into the substrate to decompose the polyester resin and the resultant high degradation temperature stimulates the formation of the intumescent char due to the existence of APP. However, for the CCA sample, besides the positive effect due to the layer structure of clay, an ablative reassembling of the silicate layers from clay can hinder NH_3 from swelling which has a negative effect on the formation of the intumescent char.[16] It can be seen that all the samples seem to have the same decomposition rate during the major mass loss period (300–450°C). However, if one considers the fact that CNF and xGnP particles are extremely stable (i.e., the exaggerated denominator for the decomposition rate of resin that containing hybrid nanopaper), it is reasonable to conclude that the introduction of hybrid nanopaper indeed increases the decomposition rate of resin which also explains why the paper-coated sample has shorter ignition time.

Post fire mechanical properties

Since the samples exposed to heat flux for more than 150 s delaminated and their mechanical resistances were very low, the mechanical tests were

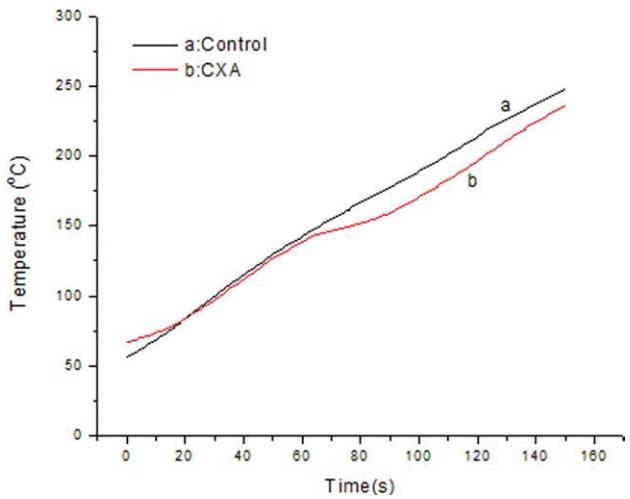

Figure 14 Unexposed surface temperature of the samples. [Color figure can be viewed in the online issue, which is available at wileyonlinelibrary.com.]

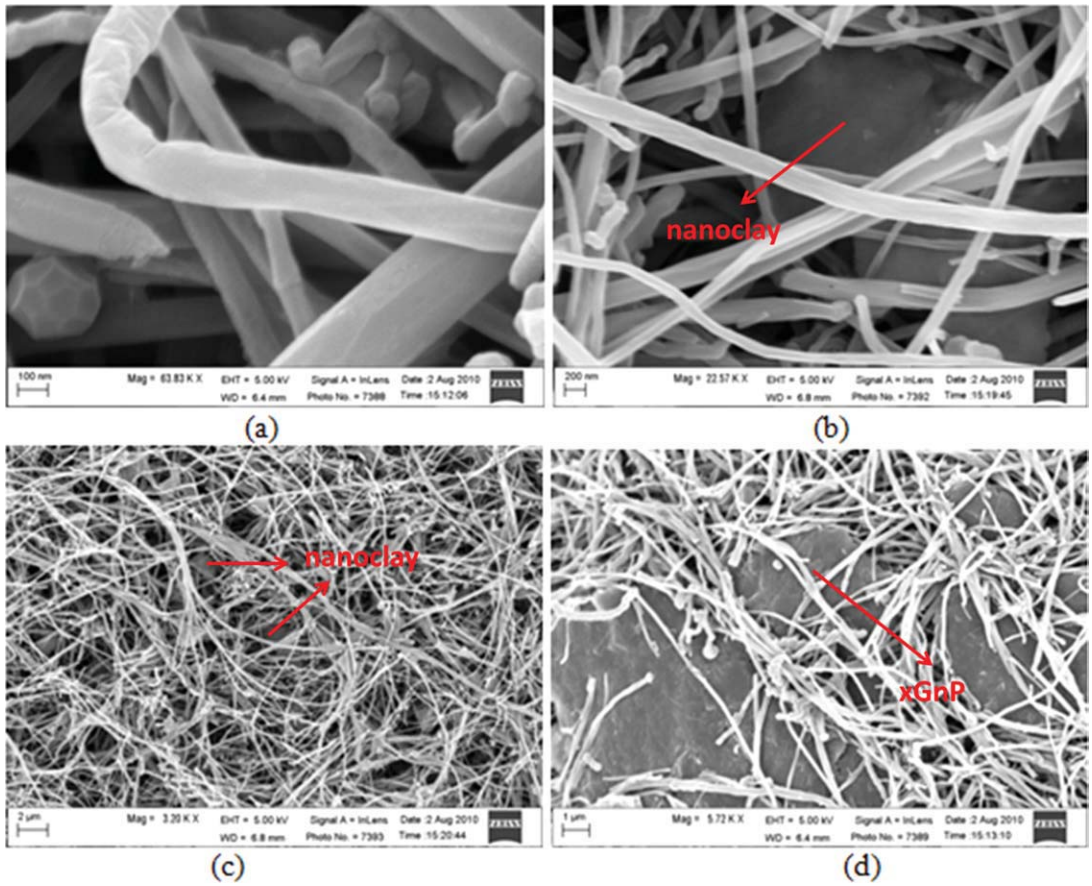

Figure 15 Hybrid nanopapers: (a) morphology of nanofibers; (b) nanoparticles within the nanofiber networks; (c) CNF/Clay/APP hybrid nanopaper; (d) CNF/Clay/xGnP hybrid nanopaper. [Color figure can be viewed in the online issue, which is available at wileyonlinelibrary.com.]

only conducted for the samples with exposure time of 0, 20, 60, 100, and 150 s in accordance with ASTM D790-10. The post-fire mechanical properties of these composite samples are shown in Figure 12.

It can be seen that the decrease rate in elastic modulus of the samples coated with hybrid nanopapers is lower than the control sample both at the early stage (before 100 s) and through overall period. The reductions in elastic modulus before 100 s for the Control, CCA and CXA samples are 54, 35, and 25%, respectively, indicating the samples coated with hybrid nanopapers exhibit more than 20% improvement in mechanical resistance during the early stage of combustion. The greater improvement in the CXA samples can be attributed to the fact that they have remarkably lower heat release rate during the major decomposition period, as shown in Figure 5. The overall decrease in elastic modulus for the Control, CCA, and CXA samples are 97, 85, and 84%, respectively. The curves that connect the data points were generated by Boltzmann Fit.

Figure 13 shows the mechanical resistance of the samples with exposure time of more than 150 s. As shown in Figure 13, the control sample cannot sustain its own weight after an exposure time of 200 s, while the samples coated with the nanopapers can sustain their own weight even after 300-s exposure. The observation confirms that the hybrid nanopapers have effectively retained the mechanical properties of FRP during fire scenario. Furthermore, even though the paper-coated samples are completely turned into char, the self-weight sustaining ability indicates that the samples still have mechanical resistance. However, the two layers model would claim that the mechanical resistance is zero in this case. Therefore, a more accurate assumption is needed to modify the model.

Temperature profiles of back surface of the samples during cone test

To further understand the reason for the different mechanical resistance degradation rate and since the CCA samples and CXA samples have similar fire performance, the temperature history of the unexposed surface of only the CXA series samples during cone treatment was recorded. Figure 14 shows the unexposed surface temperature of the samples between 0 and 150 s. As shown in Figure 14, the overall unexposed surface temperature of the sample coated with the CXA nanopaper

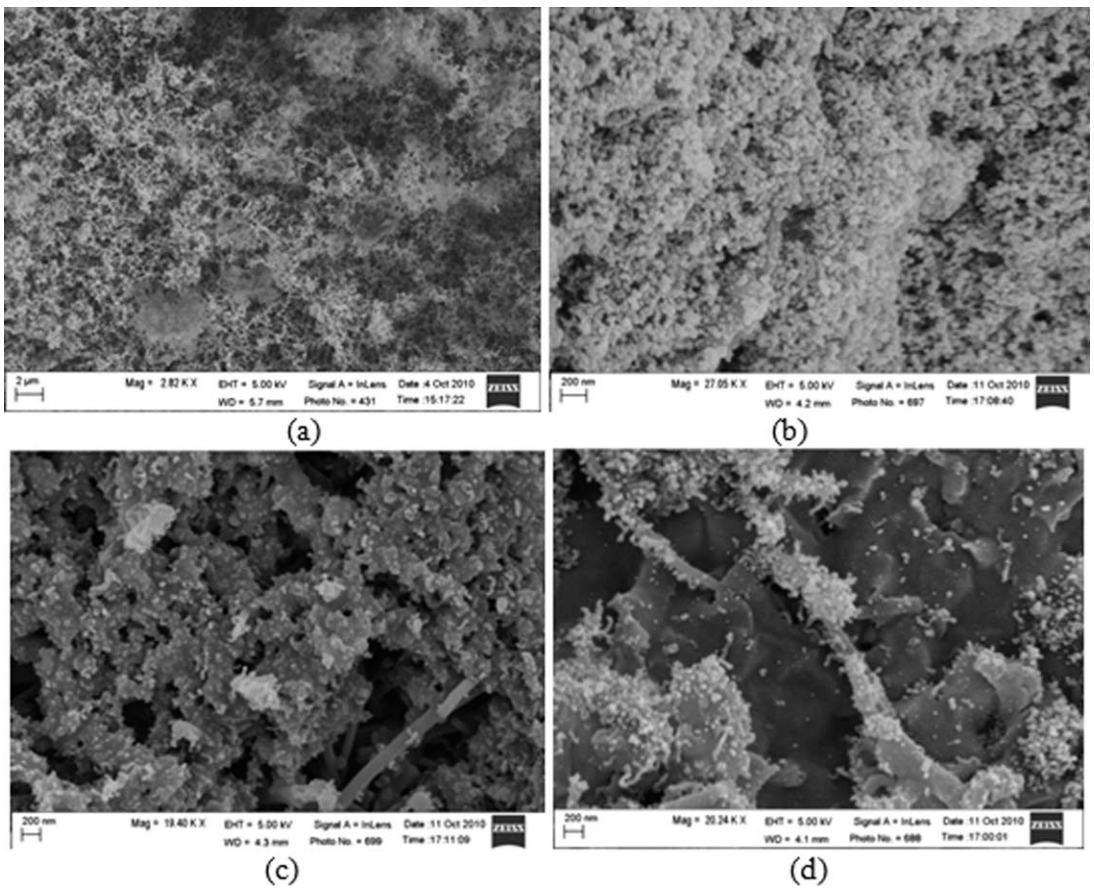

Figure 16 Morphology of different types of char: (a) top surface char structure of all samples; (b) back surface char structure of both types of nanopapers; (c) and (d) back surface char structure of CCA nanopaper.

is much lower than the control sample with the average temperature of the control sample being roughly 10% higher after 100 s of exposure. Since the mechanical properties of polymers strongly depend on the temperature, the lower temperature profile of the sample coated with the CXA nanopaper indicates better mechanical property retention, which was previously demonstrated by the bending test.

Morphology of the nanopapers and char materials

Figure 15(a–d) show the morphology of the nanofibers and hybrid nanopapers with the scale bar of 100 nm, 200 nm, 2 μm, and 1 μm, respectively. As shown in Figure 15(a), nanofibers are entangled with each other and the average diameter of nanofibers is about 80 nm. Figure 15(b) shows that the particles fit within the network structure of nanofibers so that the permeability of the nanopaper will be reduced. The morphology of hybrid nanopapers show in Figure 15(c,d) indicate that the nanofibers and particles are well dispersed without aggregation.

Figure 16 shows the morphology of different types of char obtained from the samples. The scale bar for the first image is 2 μm and for the rest of images is 200 nm. The char indicated in Figure 16(a) is the only type of char that appeared in the top surfaces of all the samples. It comes from the deposition of burnt gas and is very loose. Figure 16(b) shows the type of char that appears in both the back surfaces of the CXA and CCA nanopapers. Figure 16(c,d) show the types of char that appear only in the back surfaces of the CCA nanopapers. Type (c) and (d) are more compact than type (b) char, which is due to the low permeability of the CCA nanopapers; the morphology of the char also explains why the FRP samples coated with the nanopaper tends to build up pressure underneath the coating.

Figure 17(a,b) shows the morphology of glassfiber after the paper-coated sample is exposed to heat flux for 200 s. It can be seen that the undecomposed resin is still attached to the surface of glassfiber which retains the mechanical properties of the sample. It is reasonable to conclude that there is a directly proportional relationship between the amount of undecomposed resin retention and the elastic modulus of the sample and by extension, the efficiency of the nanopaper. In addition, compared with the glass fiber of the control sample which has no bending resistance, the residue of the resin attached to the surface of glass fiber indicates an error associated with the two layer

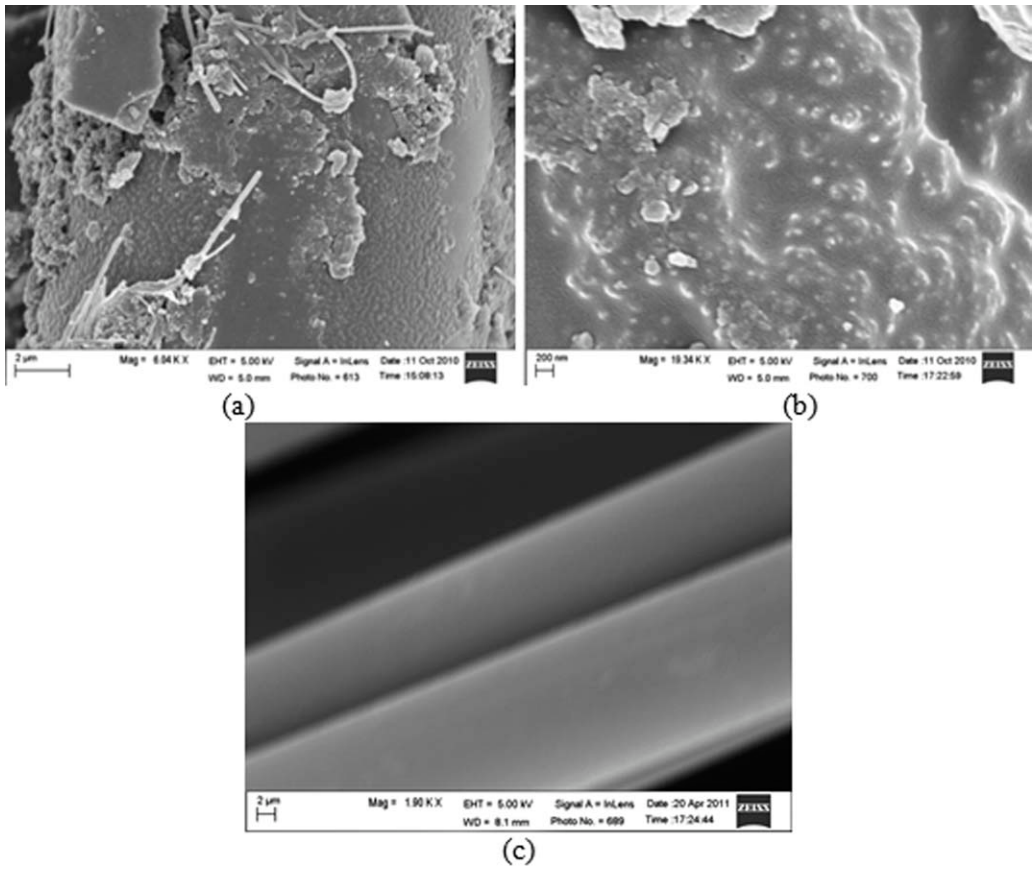

Figure 17 Morphology of the glass fiber of the sample coated with hybrid nanopaper (a) 2 μm; (b) 200 nm, and the control sample (c) 2 μm after cone test (200s).

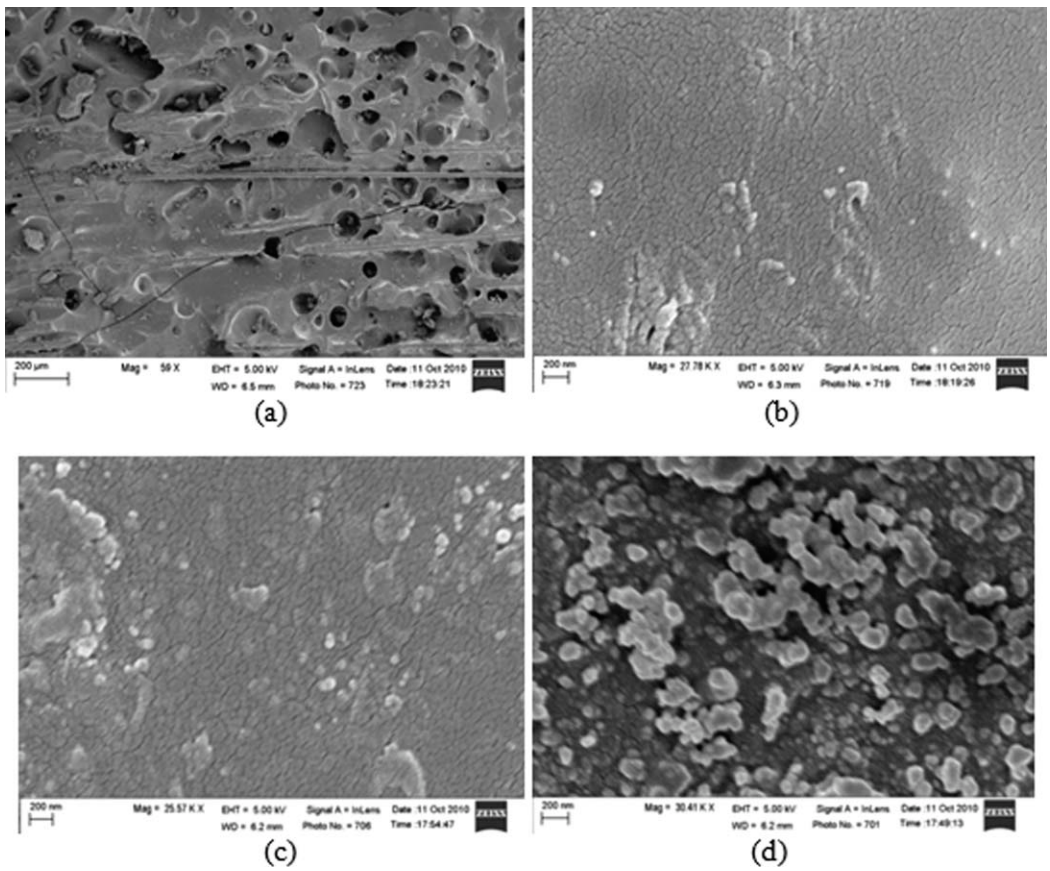

Figure 18 Morphology of the resin: (a) back of the sample with exposure time of 150 s and scale bar of 200 μm; (b) back of the sample with exposure time of 150 s and scale bar of 200nm; (c) virgin resin with scale bar of 200 nm; (d) front surface of the control sample with ignition time of less than 5 s.

model mentioned above where the mechanical resistance of the charred materials is neglected.

Figure 18 shows the morphology of virgin, degraded, and burnt resin. It is interesting to note that even though the back of the FRP sample has been severely degraded, the microscopic structure of the resin is similar to the virgin resin and is quite different from the resin that is even slightly burnt.

CONCLUSIONS

Hybrid nanopapers containing CNF/Clay/APP or CNF/xGnP/APP were fabricated and coated onto the surface of FRP. Their effect in improving the fire resistance of FRP was evaluated. The test results indicate that the hybrid nanopaper effectively reduced the heat release rate and mass loss of the composite samples. The peak heat release rate (PHRR) of the CCA and CXA samples in the major decomposition period are 23 and 34% lower than the control samples. The time to reach this PHRR for the CCA and CXA samples is roughly 125% longer than the control samples. However, even though the CCA nanopaper has much lower permeability than the CXA paper, the extremely low permeability is not necessary preferable for fire retardancy due to the fact that the CCA paper tends to detach from the underlying structure because of the built-up pressure underneath the nanopaper. Although the sample coated with the CCA paper has lower HRR than the CXA during the initial period of combustion, the CXA sample exhibit the lowest HRR in the most of the combustion period.

Bending tests indicate the post-fire mechanical properties of FRP have been enhanced with the hybrid nanopapers coating onto the surface. As a result, the samples coated with hybrid nanopapers exhibited more than 20% improvement in mechanical resistance during the early stage of combustion. The overall decrease in elastic modulus for the Control, CCA, and CXA samples are 97, 85, and 84%, respectively. Temperature profiles of the unexposed surfaces of the composite samples show that the samples retain better mechanical property exhibit with lower back surface temperature. The SEM images of the char materials suggest that the compact char layer under the nanopapers result in an improvement in fire performance and post-fire mechanical properties. Furthermore, the SEM images of glass fiber after cone calorimeter test indicate that the mechanical properties of the charred material gradually degrade.

Any opinions, findings, and conclusions or recommendations expressed in this material are those of the authors and do not necessarily reflect the views of Office of Naval Research and National Science Foundation.

References

1. Morgan, A. B.; Wilkie, C. A.; Flame retardant polymer nanocomposites. Wiley-Interscience: Hoboken 2007.
2. Nelson, G. L.; Wilkie, C. A. Fire and polymers: Materials and solutions for hazard prevention. American Chem Society: Washington, DC 2001.
3. Tjong, S. C. Mater Sci Eng R 2006, 53, 73.
4. Gojny, F. H.; Wichmann, M. H. G.; Fiedler, B.; Schulte, K. Compos Sci Technol 2005, 65, 2300.
5. Gojny, F. H.; Wichmann, M. H. G.; Fiedler B.; Schulte, K. Compos Sci Technol 2006, 66, 3115.
6. Kashiwagi, T.; Du, F.; Douglas, J. F.; Winey, K. I.; Harris, R. H. Jr.; Shields, J. R. Nature Materials 2005, 4, 928.
7. Springer, G. S. J Reinforc Plast Compos 1984, 3, 85.
8. Keller, T.; Tracy, C.; Zhou, A. Compos A 2006, 37, 1286.
9. Pering, G. A.; Farrell, P. V.; Springer, G. S. J Compos Mater 1980, 14, 54.
10. Mouritz, AP.; Mathys, Z. Compos Struct 1999, 47, 643.
11. Mouritz, AP.; Mathys, Z. Compos Sci Technol 2001, 61, 475.
12. Gou, J.; Tang Y.; Zhuge, J.; Zhao, Z.; Chen, R.; Hui, D.; Ibeh, C. Compos B 41: 176 2010.
13. Tang, Y.; Zhuge, J.; Gou, J.; Chen, R.; Ibeh, C.; Hu, Y.; Polym Adv Technol 2010; DOI: 10.1002/pat. 1621.
14. Zhuge, J.; Tang, Y.; Gou, J.; Chen, R.; Ibeh, C.; Hu, Y.; Polym Adv Techn 2010; DOI: 10.1002/pat. 1753.
15. Drzal L. T.; Fukushima, H.; Do, I.; Exfoliated grahite nano platelets (xGnP): A carbon nanotube alternative for modifying the properties of polymers and composites. XG Sciences. 2006.
16. Tang, Y; Zhuge, J.; Lawrence, J.; Mckee J.; Gou, J.; Ibeh, C.; Hu, Y. Polym Degrad Stab 2011, 92, 760.
17. ASTM D790–10 Standard test methods for flexural properties of unreinforced and reinforced plastics and electrical insulating materials.